*Research Paper*
*Computational Methods for Differential Equations*
http://cmde.tabrizu.ac.ir
Vol. *, No. *, *, pp. 1-13
DOI:10.22034/cmde.2026.67556.3226

# Influence of Activation Energy on Chemically Reacted MHD Mixed Convective Blood-Based HNF flow using BVP5C Shooting Method on a Porous Stretching Cylinder

**Chundru Maheswari[1,*], Ravuri Mohana Ramana[2], Bhavanam Naga Lakshmi[3], Jorige Girish Kumar[4], Varanasi Srinivas Bhagavan[5], and Kodi Raghunath[6]**

[1]Department of Mathematics, Vasireddy Venkatadri International Technological University, Nambur, Andhra Pradesh, India.

[2]Department of Mathematics, Narasaraopeta Engineering College (Autonomous), Narasaraopet, Andhra Pradesh, India.

[3]Department of BS & H, Vignan's Nirula Institute of Technology and Science for Women, Guntur, Andhra Pradesh, India.

[4]Department of Mathematics, Government Degree College (Autonomous), Nagari, Andhra Pradesh, India.

[5]Department of Engineering Mathematics, Koneru Lakshmaiah Education Foundation, Guntur, Andhra Pradesh, India.

[6]Department of Humanities and Sciences, St. Johns College of Engineering and Technology (Autonomous), Yemmiganur-518360, Andhra Pradesh, India.



**Abstract**

This study investigates the mass and heat transfer characterisations of a two-dimensional, steady-state, axisymmetric, incompressible, MHD, laminar hybrid ($Au-Cu/Blood$) nanofluid flow over a permeable porous stretched cylinder. The analysis considers various governing parameters, including the mixed convective parameter ($0.1 \leq \lambda \leq 5$), concentration to thermal buoyancy ratio parameter ($0 \leq N \leq 8$), activation energy ($1 \leq E \leq 3$), chemical reaction parameter ($1 \leq Rc \leq 9$), curvature parameter ($0 \leq \gamma \leq 4$), Hartmann number ($0 \leq Ha \leq 20$), Darcy number ($1 \leq Da \leq 9$), heat source or sink parameter ($-0.2 \leq Q \leq 0.2$), radiation parameter ($1 \leq Rd \leq 5$) and Eckert number ($0.1 \leq Ec \leq 0.5$). Tiwari-Das model is utilized to analyse the flow dynamics. Since blood exhibits Newtonian properties in arteries, large cavities and veins, this study assumes blood to be a Newtonian fluid with a Prandtl number of 21. A key innovation of this research is the application of the prescribed heat flux with thermal boundary constraint. Non-linear PDEs generate ODEs by employing similarity transformations. Numerical solutions are derived using BVP5C method in MATLAB, utilizing an approach of shooting technique. This study reveals that the velocity rises with progressive values of $\lambda, N$ and $\gamma$, whereas an inverse trend is noticed with increasing $Ha$ and $Da$. The temperature progresses, the hiking of $\gamma, Ha, Da, Rd, Ec$ and $Q$, trend is opposite for $\lambda$. The profile of concentration enhancing in $E, \gamma$ hiking, while the trend is opposite for enhancing the $\lambda, N, Rc$ and $Sc$. This work also exposes that as $\lambda$ increases from 0.1 to 0.7, heat transmission rate and skin friction constant rise by 30% and 27% respectively, while the mass transfer rate declines by 8%. When $E$ ranges from 1.0 to 2.5, heat and mass transmission rate, the skin friction constant exhibit slight increases of 0.1%, 1.4% and 0.1% respectively. As $Rc$ varies from 1 to 7, reductions of 3%, 3.4% and 57% are observed in the skin friction constant, heat and mass transmission rate respectively. Accuracy of this model has been rigorously validated against existing data, demonstrating excellent reliability.

**Keywords.** Au-Cu/Blood hybrid nanofluid, Mixed convection, Chemical reaction, Activation energy, Joule heating, Viscous dissipation.
**2010 Mathematics Subject Classification.** 76A05, 76S05, 76W05, 76D05.

## 1. Introduction

The integration of two different types of nano-particles into a base fluid generates a hybrid nanofluid. When the nanoparticles are effectively dispersed, hybrid nanofluids provide remarkable benefits, including exceptionally high thermal conductivity. Moreover, hybrid nanofluids exhibit greater viscosity compared to traditional fluids and many single-component nanofluids, although this depends on the specific nanoparticles and their combinations[48]. They

Received: 28 May 2025; Accepted: 28 July 2026.
∗ Corresponding author: cmaheswari2014@gmail.com.

also possess superior rheological properties and are less likely to cause pipe clogging. Owing to their excellent heat transfer capabilities, hybrid nanofluids are widely utilized in Biomedical Engineering, Industrial applications and Manufacturing [35]. Their large surface area and significant absorption capacity make hybrid nanoparticles valuable across various fields, such as Medicine (general healthcare, drug delivery, genomics, surgery, pharmacogenomics and optics); Agriculture (prosthetics and tissue engineering); Industry (textile technology and energy); and environmental science (physical and health sciences) [51, 54]. Cooling rates vary depending on the hybrid nanofluids' viscosity and the specific geometric configuration through which they flow [15]. Cylindrical shapes play a vital role in heat transfer due to their different applications, including emulsion production, hot rolling, fabric production, photographic films, metallurgy, petroleum ships, copper wire thinning, paper production, crude oil refinement, polymer extrusions and metal shaping [25]. The efficiency of final products and the expenses involved in production are closely linked to mass and heat transmission rates. As a result, studying the flow of boundary layer, as well as mass and heat transmission over a stretched cylinder has become a topic of significant curiosity [5]. Flow around a cylinder is typically treated as two-dimensional. However, when the radius of cylinder correlates to the thickness of the boundary layer, the flow can be regarded as axi-symmetric. Consequently, the leading equations contain the transverse curvature term, plays a crucial role in influencing the temperature, velocity and concentration distributions [41]. Studying fluid's flow in flexible cylindrical geometries is a key concentration in fluid mechanics, driven by their wide use in biomedicine, engineering and industry. These applications range from drug delivery, cancer treatment, MRI, turbine systems, jet propulsion and data storage technologies [27]. Magnetohydrodynamics (MHD) is the study of the magnetic properties and behavior of electrically conductive liquids. These magneto-liquids contain plasma, electrolytes, fluid metals and saltwater. The essential principle of MHD liquid is that magnetized fields can produce currents in a flowing conducting liquid, leading to the polarization of the liquid. This interaction modulates the magnetic field, which affects the fluid dynamics [29]. By applying magnetic fields and leveraging the distinctive properties of nanofluids, including their improved electrical and thermal conductivity, researchers can achieve precise control over heat transfer and fluid flow. This interdisciplinary approach merges fluid dynamics, electromagnetism and nanotechnology, paving the way for ground-breaking applications in cooling systems, medical treatments, materials processing and power generation. Magnetic fields are crucial in convection processes involved in materials manufacturing, nuclear reactor control and metal casting [31]. Over the past few decades, the research on liquid flow and heat transmission within porous medium has captured the consideration of many scholars. This heightened interest is primarily driven by the extensive range of industrial applications, like compact heat exchangers, thermal insulation, electronic devises cooling, petroleum engineering and subsurface energy structures [16]. Thermal radiation is heat transmission form that works using electromagnetic waves, finding practical uses in various fields such as rocket propulsion, polymer processing and gas turbines [2, 10, 38]. In 1840, Joule introduced the notion of Joule heating [24], where heat is created when an electric current passes from a resistivity material, also acknowledged as Ohmic heating. This concept has been widely studied for its applications in heat transfer. Joule heating is commonly utilized in stoves, electric boilers, cooking appliances, resistance ovens, industrial progressions and numerous heating elements, to transform energy from electricity into thermal energy. It also plays a crucial role in electrical systems by preventing overheating of components in high-current situations [26]. Viscous dissipation refers to the rate at which kinetic energy transmuted into thermal energy in a viscous fluid per unit of mass [37]. It is a crucial factor in heat transfer around a stretching cylindrical pipe, significantly influencing the thermal behavior of fluids over heated surfaces. Although often neglected, the effects of viscous dissipation become vital when viscosity of fluid is in elevation. It modifies thermal circulations by serving as an internal energy source, leading to fluctuations in heat transfer concentrations [18]. Many researchers have sightseen the diverse impressions on the fluid flow, (hybrid) nanofluids on a stretched cylinder. Sadighi et al. [42] carried out innovative research on parametric solutions to energy and the Navier-Stokes equations. Their study emphasized heat transmission and fluid flow, considering the influences of a Joule heating, magnetized field, heat absorption/generation, viscous dissipation and thermal radiation. They uniquely applied the prescribed heat flux (PHF) thermal boundary layer condition to a permeable stretched cylinder in their analysis. The same authors in [43] carried out a parametric investigation of mass and heat transmission in a two-dimensional, laminar, steady-state flow of $Fe_3O_4 - H_2O$ nanofluid. Their study considered various influencing factors, including thermal radiation, inclined magnetic field, electrical resistance heating, curvature, chemical reactions, viscous dissipation and power-law exponent effect. Abbas et al. [1] examine the hybrid nano-liquid flow with stagnation point subjected to the field of inclined magnet on a moving cylinder. Their study utilizes the extension forms of Yamada-Ota and Xue models for hybrid nanofluids, applying the BVP-4C technique to conduct the analysis. Awan et al. [6] performed a computational and theoretical analysis of Ellis hybrid nanofluid ($AA7072-AA7075/H_2O$) flow model. Their study included the effects of magnetic field, non-linear thermal radiation, Darcy-Forchheimer drag on the flow over a stretched cylinder, applying slip in BC of cylinder. Ali et al. [3] scrutinised the impact of non-uniform heat flux and thermal radiation on the magneto-hydrodynamic $CuO - Fe_2O_3$/water hybrid nanofluid flow over a stretchable cylinder. Their analysis included the application of velocity slip conditions to investigate the slippage effect and they observed that the field effected by magnet is insignificant when assuming a low Reynolds number. Li et al. [28] examined two distinct hybrid nano-liquid thermal flow properties, that impact obliquely on a stretchy cylinder. Their study considered base fluid as $FC - 77$ and water-ethylene glycol mixture and SWCNTs and MWCNTs as nanoparticles. Blood, the fluid that circulates throughout the body, plays a crucial role in the development of cardiovascular disorders. In recent decades, the use of computational simulations and mathematical modelling in Hemodynamics has significantly expanded to enhance the awareness of the underlying reasons of various illnesses and to discover advanced treatments for their prevention [49]. Blood exhibits intricate macroscopic behaviour caused by the characteristics of its components and overall constitution. When the shear rate exceeds $100s^{-1}$, blood typically acts like a Newtonian fluid. Conversely, at shear speeds below $100s^{-1}$, it demonstrates non Newtonian behaviour. Blood veins are essential parts of the circulation system. The main function of this circulatory system is to deliver vital nutrients and oxygen to healthy tissues throughout the body while eliminating waste materials. Blood flow dynamics significantly contribute in the creation and progression of cardiovascular illnesses that are the primary cause of death in underdeveloped countries [21].

Bio-nanofluids represent a relatively new area of research in biomedicine and have garnered significant attention owing to its potential uses in targeted delivery, diagnostics and imaging. In particular, the utilization of Bio nanofluids in the context of human blood has attracted considerable interest, because these fluids possess the ability to increase the delivery of medications and other therapeutic agents inside the circulation system [11]. Presence of nanomaterials in bio liquids may enhance the liquid's viscosity and alter the blood vessel walls surface properties, affecting the way they interact with neighbouring cells and the walls of blood artery vessels. Furthermore, bio-nanoliquids may enhance the solubility and bioavailability of medicines and therapeutic agents, thereby increasing their effectiveness and reducing side effects. Bio-nanoliquids are used to improve flow of blood in various applications. For instance, it has been demonstrated that incorporating nanoparticles, such as gold or copper, into blood can reduce its viscosity and enhance circulation [4]. Thermal properties of bio-nanoliquids, have captured the attention of researchers because of its application in nanotechnology and medical treatments, like hyperthermia, MRI, MHD micro-pump, biomedical sensors and nano-cryosurgery [7]. Nanotechnology has introduced a ground-breaking area of science with numerous applications. By meticulously examining different materials and their properties, novel characteristics have been observed when these materials are transformed into nanoparticles. These newfound properties hold significant medical importance, particularly in treatment applications [36]. Copper and gold nanoparticles hold significant importance in the fields of nanomedicine and nanoscience. They play various roles, including serving as photovoltaic agents, drug delivery systems, wound treatment, cardiovascular treatment, cancer diagnosis, chemotherapy contrast agents, and tools for radio-based therapies. Additionally, their unique properties make them highly desirable for applications in biomedical diagnostics and treatments [19]. Gold ($Au$) nanoparticles have received substantial attention because of their unique ability for interaction with light via SPR (surface plasmon resonance) [55]. They have been extensively explored as a promising tool for cancer diagnosis and treatment, AIDS therapy, antibacterial applications, medication delivery and bio-imaging. The non-toxic and immunogenic character of $Au$ nano-particles, combined with their substantial permeation and enhanced retention impact, additionally facilitates their effective accumulation and penetration at tumour sites, making them highly suitable for targeted tumour treatments [52]. Copper ($Cu$) nanoparticles are widely used in biomedicine, primarily for their strong antibacterial features. These capabilities make them useful for situations such as coatings for medical implants, wound dressings and combating bacterial infections, especially those produced by resistant to antibiotics. Furthermore, ongoing research is investigating their potential in cancer therapy, drug delivery systems, and bio-sensing, leveraging their unique features like controlled ion release and interactions with biological molecules [8]. Convection is divided into two distinct types: free (natural) convection and forced convection. Mixed convection flow describes a type of fluid motion where both forced convection, driven by an external pressure gradient and free convection, driven by buoyancy forces, occur simultaneously [30]. The behaviour of mixed convection flow along a stretched geometry has numerous uses in industry and engineering. Under the influence of forces of gravitation, the effect of free convection becomes increasingly significant. Both stretching forces and buoyancy forces play a critical role in governing flow and heat transmission devices. Thermal buoyant arises when fluctuations in temperature occur on the stretched region, impacting heat transfer rates in various industrial operations [46]. This phenomenon influences extensive range of applications, including electronic devices cooling, low-velocity heat exchangers, crystal growth, underground cable systems, chemical processing, lubrication technologies, boilers, emergency cooling of nuclear reactors, solar energy systems, defroster systems, atmospheric flows, vehicle demisters and oceanic flows [53]. Das et al. [12] reviewed nanofluid's flow combined with convection flow on an inclined stretched cylinder, considering the effects of heat radiation and magnetic fields. Mondal et al. [34] conducted an analysis of constant, viscous $2-D$ MHD mixed convicted nanofluid flow and heat transmission around an inclined stretched cylinder, incorporating the impacts of homogeneous magnetic field and chemical reaction. Roy et al. [40] examined the magnetic hybrid nanofluid's flow mixed convection behavior on a contracted cylinder embedded in a medium with pores. Analysing flow of fluid with chemical reactions is essential because of its significant impact on environmental and industrial processes. Chemical reactions are crucial in various fields, including nuclear reactors, atomic energy production, plastic manufacturing, cable production, and numerous other industrial applications [32]. In 1889, Svante Arrhenius coined the term activation energy while analysing mass and heat transmission progressions. According to him, activation energy is the bare minimum of energy needed to initiate chemical processes. Activation energy represents the threshold energy required to trigger chemical reactions in large-scale oil reservoirs, solar energy generation, and health care and food production. By applying the concept of activation energy, industrial sectors can enhance process control, boost revenue and gain a competitive edge in their respective markets [39]. Souayeh et al. [47] explored hybrid nanofluid's flow in a uniform peristaltic channel, considering various factors such as EMHDs, thermal radiation, gyrotactic micro-organisms and activation energy. Guo et al. [17] examined hybrid nanofluid ($Al_2O_3 - Ag/water$) heat and mass transmission over a perpendicular cylinder, incorporating slip and convicted boundary conditions, non-linear radiation, activation energy and viscous dissipation. Imoro et al. [22] explored chemically reacted MHD blood-based hybrid nanofluid's flow containing Ag and Cu nanoparticles through a stenosed artery. Basha et al. [9] investigated fluid transit characteristics of Cu - Au/bio-magnetic blood-based hybrid nanofluid's flow in an inclined vein with irregular stenosis, considering the influence of Lorentz force and fluctuating viscosity. Shahzad et al. [45] explored how magnetic forces influence velocity and temperature profiles with the flow of pulsatile over a cylinder duct. Similarly, Uma Devi et al. [50] studied the effects of magnetic forces on the flow of blood, using a copper nanoparticle suspension in water. To investigate fractional-order partial differential equations, Jassim et al. [23] adopted a hybrid strategy known as the homotopy analysis Sumudu transform method, formed by merging the Sumudu transform with the homotopy analysis method. Based on the reviewed literature, it is evident that the analysis of mixed convective hybrid nanofluid $Au - Cu/Blood$, incorporating the influences of activation energy, chemical reaction, Joule heating, viscous dissipation, Schmidt number, Hartmann and Darcy numbers, curvature parameter, Eckert number, radiation and heat sink or source parameters over a stretching porous cylinder remains unexplored. The novelty of this investigation lies in addressing the existing gap by investigating the key parameters in this study. These include the chemical reaction; the ratio of concentration-to-thermal buoyancy forces; activation energy; mixed convection, radiation, heat source/sink and curvature parameters; Eckert, Hartmann, Schmidt and Darcy numbers. Their effects on the temperature, velocity and concentration distributions of the hybrid nanoliquid ($Au - Cu/Blood$) over a porous stretched cylinder are thoroughly analysed. A key innovation of this work is the application of the prescribed heat flux (PHF) thermal boundary constraint for a permeable stretched cylinder. Similarity transformations are utilized to transform non-linear PDEs into non-linear ODEs. Numerical solutions are computed utilizing the BVP-5C method in MATLAB, employing a shooting strategy. The effects of physical parameters are analysed and displayed in the form of tables and figures. Comprehensive validation against previously published data highlights the correctness and model's reliability.

## 2. Problem's formulation

This work examines the behaviour of a two-dimensional, axisymmetric, steady-state, incompressible, viscous, laminar MHD $Au-Cu/Blood$ hybrid nanofluid flowing over a permeable porous stretched cylinder, having radius $R$, under the influence of body forces. Figure 1 illustrates the permeability cylinder expanded along the $x$-direction while a transverse magnetic field is applied to the electrically conductive fluid across the $r$-axis. The velocity of the permeable stretched cylinder follows a linear variation, expressed as $u_w(x) = \frac{ax}{l}$, where, $a$ represents a positive constant and $L$ denotes the characteristic length. This study considers blood as its base fluid and assumes it behaves like a Newtonian fluid, as it displays Newtonian characteristics in large cavities, veins, and arteries. Initially, a nanofluid composed of $Cu - Blood$ is prepared by dispersing copper ($Cu$) nanoparticles with a volume fraction represented by $\phi_1$ into the blood. This nanofluid is then further refined into a Au-Cu/Blood hybrid nanofluid by adding gold ($Au$) nanoparticles, with a high thermal conductivity and a specified volume fraction $\phi_2$ into the existing $Cu-Blood$ nanofluid. Similarity transformations are utilized to transform non-linear PDEs into non-linear ODEs. Numerical solutions are computed utilizing the BVP-5C method in MATLAB, employing a shooting strategy.

Based on the preceding considerations and employing the Tiwari-Das model [42], the governing two-dimensional

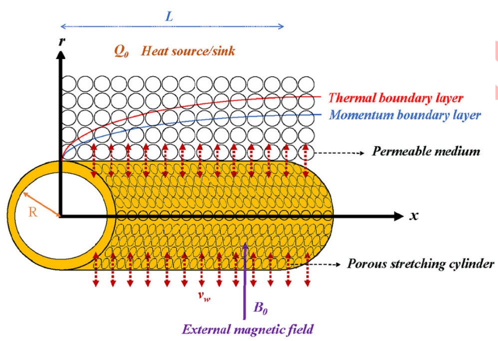


Figure 1. Problem's Geometry[42].

nonlinear PDEs for momentum, continuity, energy and concentration are derived as follows [1, 42, 43]:

$$\frac{\partial}{\partial x}(ru) + \frac{\partial}{\partial r}(rv) = 0, \tag{2.1}$$

$$u\frac{\partial u}{\partial x} + v\frac{\partial u}{\partial r} = \frac{\mu_{hnf}}{\rho_{hnf}}\left(\frac{\partial^2 u}{\partial r^2} + \frac{1}{r}\frac{\partial u}{\partial r}\right) - \frac{\sigma_{hnf}}{\rho_{hnf}}B_0^2 u - \frac{\mu_{hnf}}{\rho_{hnf}}\frac{1}{K_0}u + g\left[\beta_T(T - T_\infty) + \beta_C(C - C_\infty)\right], \tag{2.2}$$

$$(\rho C_p)_{hnf}\left(u\frac{\partial T}{\partial x} + v\frac{\partial T}{\partial r}\right) = k_{hnf}\left(\frac{\partial^2 T}{\partial r^2} + \frac{1}{r}\frac{\partial T}{\partial r}\right) - \frac{\partial}{\partial r}(q_r)$$
$$+ \mu_{hnf}\left(\frac{\partial u}{\partial r}\right)^2 + \sigma_{hnf}B_0^2 u^2 + \mu_{hnf}\frac{1}{K_0}u^2 + Q_0(T - T_\infty), \tag{2.3}$$

$$u\frac{\partial C}{\partial x} + v\frac{\partial C}{\partial r} = D_B\left(\frac{\partial^2 C}{\partial r^2} + \frac{1}{r}\frac{\partial C}{\partial r}\right) - K^{'}\left(C - C_\infty\right)\left(\frac{T}{T_\infty}\right)^n exp\left(\frac{-E_a}{K_a T}\right). \tag{2.4}$$

The subsequent boundary constraints, including a thermal boundary condition with prescribed heat flux [1, 42, 43]:

$$u = u_w(x) = \frac{ax}{L},\ v = v_w,\ C = C_w,\ q_w = A\left(\frac{x}{L}\right)^2\ at\ r\ =\ R, u \to 0,\ T \to T_\infty,\ C \to C_\infty\ as\ r \to \infty. \tag{2.5}$$

Here $v$ and $u$ represent the velocity in the $r$ and $x$- directions; $T$ and $C$ are the fluid temperature and concentration respectively; and $A$ is a constant. While considering the stagnant part, $\mu_{hnf}$ (viscosity), $(\rho C_p)_{hnf}$ (heat capacity),

TABLE 1. Thermophysical properties of $Au-Cu$/Blood hybrid nanofluid.

| **Property** | **Expression** |
|---|---|
| Viscosity ($\mu$) | $\mu_{hnf}=\dfrac{\mu_f}{(1-\phi_1)^{2.5}(1-\phi_2)^{2.5}}$ |
| Density ($\rho$) | $\rho_{hnf}=[\{(1-\phi_1)\rho_f+\phi_1\rho_{s_1}\}(1-\phi_2)]+\phi_2\rho_{s_2}$ |
| Heat capacity ($\rho C_p$) | $(\rho C_p)_{hnf}=(1-\phi_2)\{(1-\phi_1)(\rho C_p)_f+\phi_1(\rho C_p)_{s_1}\}+\phi_2(\rho C_p)_{s_2}$ |
| Thermal conductivity ($k$) | $\dfrac{k_{hnf}}{k_{bf}}=\dfrac{ks_2+2k_{bf}-2\phi_2(k_{bf}-ks_2)}{ks_2+2k_{bf}+\phi_2(k_{bf}-ks_2)}$, where $\dfrac{k_{bf}}{k_f}=\dfrac{ks_1+2k_f-2\phi_1(k_f-ks_1)}{ks_1+2k_f+\phi_1(k_f-ks_1)}$ |
| Electrical conductivity ($\sigma$) | $\dfrac{\sigma_{hnf}}{\sigma_{bf}}=\dfrac{\sigma_{s_2}+2\sigma_{bf}-2\phi_2(\sigma_{bf}-\sigma_{s_2})}{\sigma_{s_2}+2\sigma_{bf}+\phi_2(\sigma_{bf}-\sigma_{s_2})}$, where $\dfrac{\sigma_{bf}}{\sigma_f}=\dfrac{\sigma_{s_1}+2\sigma_f-2\phi_1(\sigma_f-\sigma_{s_1})}{\sigma_{s_1}+2\sigma_f+\phi_1(\sigma_f-\sigma_{s_1})}$ |



$\rho_{hnf}$ (density), $k_{hnf}$ (thermal conductivity) and $\sigma_{hnf}$ (electrical conductivity) for $Au-Cu$/Blood hybrid nanofluid are expressed as in Table 1 [1, 20, 31, 35, 42, 43, 51]: The Roseland estimate states that the radiation flux is provided by [42].

$$q_r=-\frac{16\sigma^* T_\infty^3}{3K^*}\frac{\partial T}{\partial r}. \tag{2.6}$$

Here $K^*$ and $\sigma^*$ represents mean absorption co-efficient and Stefan-Boltzman constant. The similarity transformations are defined as [42, 43]:

$$\eta=\frac{r^2-R^2}{2R}\sqrt{\frac{a}{\nu_f L}},\qquad u=\frac{axf'(\eta)}{L},\qquad v=\frac{-R}{r}\sqrt{\frac{a\nu_f}{L}}\,f(\eta),$$
$$T=T_\infty+\frac{q_w}{k_f}\sqrt{\frac{L\nu_f}{a}}\,\theta(\eta),\qquad \phi(\eta)=\frac{C-C_\infty}{C_w-C_\infty}. \tag{2.7}$$

Following are the non-dimensional parameters [12, 17, 21, 31, 35, 42, 43, 51]:

$$Da=\frac{\mu_f L}{a\rho_f K_0},\quad Ha=\frac{\sigma_f B_0^2 L}{a\rho_f},\quad \gamma=\sqrt{\frac{\nu_f L}{aR^2}},\quad Rd=\frac{16\sigma^* T_\infty^3}{3K^* K_f},\quad \Pr=\frac{\nu_f(\rho C_p)_f}{k_f},\quad Ec=\frac{u_w^2}{(C_p)_f(T_w-T_\infty)},$$
$$Sc=\frac{\nu_f}{D_B},\quad Rc=\frac{LK'}{a},\quad Q=\frac{Q_0 L}{a(\rho C_p)_f},\quad \alpha=\frac{T_w-T_\infty}{T_\infty},\quad E=\frac{E_a}{K_a T_\infty},\quad Gr_t=\frac{g\beta_T(T_w-T_\infty)x^3}{\nu_f^2},$$
$$Gr_c=\frac{g\beta_C(C_w-C_\infty)x^3}{\nu_f^2},\quad \lambda=\frac{Gr_t}{Re_x^2}=\frac{g\beta_T(T_w-T_\infty)L^2}{a^2x},\quad N=\frac{Gr_c}{Gr_t},\quad Re_x=\frac{ax^2}{\nu_f L}. \tag{2.8}$$

In equation (2.8), the parameters $Da$, $Ha$, $\gamma$, $Rd$, $Pr$, $Ec$, $Q$, $Rc$, $Sc$, $\alpha$, $E$, $Gr_t$, $Gr_c$, $\lambda$, $N$, $Re_x$ represent, the Darcy number, Hartmann number, curvature parameter, radiation parameter, Prandtl number, Eckert number, heat source or sink parameter, chemical reaction parameter, Schmidt number, temperature ratio (or difference) parameter, activation energy parameter, thermal Grashof number, mass Grashof number, mixed convection parameter, concentration-to-thermal buoyancy forces ratio parameter and local Reynolds number respectively.
By applying the similarity transformations given in Eq. (2.7) and the non-dimensional parameters given in Eq. (2.8), Eq. (2.1) is identically satisfied and Eqs. (2.2) through (2.4) are transmuted as follows:

$$A_1(1+2\gamma\eta)f'''+A_2\left(ff''-f'^2\right)+2A_1\gamma f''-(A_3Ha+A_1Da)f'+A_2\lambda(\theta+N\phi)=0. \tag{2.9}$$

$$(1+2\gamma\eta)\left(A_4+Rd\right)\theta^{''}+\left(2A_4+Rd\right)\gamma\theta^{'}+PrA_5\left(f\theta^{'}-2f^{'}\theta\right)+PrA_1\left(1+2\gamma\eta\right)Ecf^{''^2}$$
$$+PrEc\left(A_3Ha+A_1Da\right)f^{'^2}+PrQ\theta=0, \tag{2.10}$$

$$(1+2\gamma\eta)\,\phi^{''}+2\gamma\phi^{'}+Sc\left(f\phi^{'}-m\phi f^{'}\right)-ScRc\left(1+\alpha\theta\right)^n exp\left(\frac{-E}{1+\alpha\theta}\right)\phi=0. \tag{2.11}$$

Here

$$A_1=\frac{\mu_{hnf}}{\mu_f},\ A_2=\frac{\rho_{hnf}}{\rho_f},\ A_3=\frac{\sigma_{hnf}}{\sigma_f},\ A_4=\frac{k_{hnf}}{k_f},\ A_5=\frac{(\rho C_p)_{hnf}}{(\rho C_p)_f},$$

The transformed border conditions are [42, 43]:

$$f(0)=s,\ f'(0)=1,\theta^{'}(0)=-1,\phi(0)=1.f'(\infty)\to 0,\theta(\infty)\to 0,\phi(\infty)\to 0. \tag{2.12}$$

Measuring the surface drag of the MHD $Au-Cu$/Blood hybrid nanofluid flowing, along with the mass and heat transmission rates from the porous stretching cylinder, is crucial. The problem focuses on the relevant physical amounts, $C_f$(the Skin friction coefficient), $Nu_x$(Nusselt number), $Sh_x$(local Sherwood number) [42, 43].

$$C_f=\frac{\mu_{hnf}}{\rho_f {u_w}^2}\left(\frac{\partial u}{\partial r}\right)_{r=R},\quad Nu_x=\frac{-x\left(k_{hnf}+\frac{16\sigma^* {T_\infty}^3}{3(\rho C_P)_f}\right)}{k_f(T_w-T_\infty)}\left(\frac{\partial T}{\partial r}\right)_{r=R},\ Sh_x=\frac{-D_B x}{D_B(C_w-C_\infty)}\left(\frac{\partial C}{\partial r}\right)_{r=R}.$$

The terms for the reduced $C_f$, $Nu_x$ and $Sh_x$ are as follows:

$$Re_x^{\frac{1}{2}}C_f=A_1 f''(0),\ Re_x^{-\frac{1}{2}}Nu_x=\left(\frac{k_{hnf}}{k_f}+Rd\right)\frac{1}{\theta(0)},\ Re_x^{-\frac{1}{2}}Sh_x=\phi'(0).$$

## 3. Solution method

A numerical study was conducted on the structure of nonlinear total differential Eqs. (2.9) to (2.11), along with the boundary constraints outlined in Eq. (2.12), utilizing the BVP-5C shooting technique in MATLAB. The BVP-5C scheme was selected due to its simplicity and fast convergence. By introducing supplementary variables, the coupled non-linear ODEs were converted into a structure of first-order and first degree ODEs, highlighting a significant advantage of this approach.

This method entails transforming equations (2.9)-(2.11) and their associated boundary conditions into a series of seven first-order equations. Let

$$y(1)=f,\ y(2)=f',\ y(3)=f'',y(4)=\theta,\ y(5)=\theta^{'},\ y(6)=\phi,y(7)=\phi'. \tag{3.1}$$

As a result, Eqs. (2.9)-(2.11) reduces to

$$y'(3)=\frac{1}{A_1\left(1+2\gamma\eta\right)}\left[A_2y(2)y(2)-A_2y(3)y(1)-2A_1\gamma y(3)+\left(A_3Ha+A_1Da\right)y(2)-A_2\lambda\left(y(4)+Ny(6)\right)\right], \tag{3.2}$$

$$y'(5)=\frac{1}{\left(A_4+Rd\right)\left(1+2\gamma\eta\right)}[-\left(2A_4+Rd\right)\gamma y(5)-Pr(A_5(y(5)y(1)-2y(4)y(2))+A_1(1+2\gamma\eta)Ecf(3)^2$$
$$+Ec(A_3Ha+A_1Da)f(2)^2+Qy(4))], \tag{3.3}$$

$$y'(7)=\frac{1}{(1+2\gamma\eta)}[-2\gamma y(7)-Sc(y(7)y(1)-my(6)y(2))+ScRc(1+\alpha y(4))^n exp\left(\frac{-E}{1+\alpha y(4)}\right)y(6)]. \tag{3.4}$$

With the boundary constraints

$$ya(1)=s,\ ya(2)=1,\ ya(5)=-1,\ ya(6)=1,\ yb(2)=0,\ yb(4)=0,\ yb(6)=0. \tag{3.5}$$

Here, $ya$ and $yb$ represent the functions of their corresponding dependent variables, evaluated at $\eta=0$ and $\eta\to\infty$ respectively. Eqs. (3.2) to (3.4) along with the boundary limitations outlined in Eqs. (3.5) are numerically solved

TABLE 2. Thermo-physical characteristics of gold (Au), copper (Cu), and blood [35].

| **Properties** | $Au$ | $Cu$ | Blood |
|---|---|---|---|
| $\rho(kg/m^3)$ | 19,282 | 8933 | 1063 |
| $k(W/mK)$ | 310 | 401 | 0.492 |
| $C_p(J/kgK))$ | 129 | 385 | 3594 |
| $\sigma(\Omega/m)$ | $4.1X10^6$ | $5.96X10^7$ | 0.8 |
| Pr | – | – | 21 |

utilizing the Runge - Kutta methodology combined with the BVP-5C shooting technique, implemented in the user-friendly MATLAB software, which guarantees continuity over the interval $[0, \infty]$. The method starts with preliminary guess provided at the primary grid points and adjusts the size of the step dynamically to attain the required level of correctness. The final number of grid points is determined iteratively by the BVP-5C solver as it progresses through the solution. Table 2 presents the thermophysical attributes of essential factors, including copper $(Cu)$ and gold $(Ag)$ nano sized particles, in addition to the initial fluid, blood, which perform a crucial role in defining the features of the hybrid nanoliquid. The results illustrate the impact of several dimensionless parameters, containing the concentration-to-thermal buoyancy forces ratio parameter, mixed convection parameter, activation energy, chemical reaction parameter, Hartmann number, Darcy number, heat source/sink parameter, radiation parameter, Schmidt number and Eckert number on the temperature, velocity and concentration profiles. To achieve a convergence condition of $10^{-6}$, the RK-Shooting method is repeatedly applied. The responses to this problem are presented in both graphically and table formats.

## 4. Results and discussion

This research employs the Tiwari-Das emulate to investigate the flowing characteristics, as well as mass and heat transmission, of a two-dimensional, steady, axisymmetric, viscous, laminar and incompressible magneto-hydrodynamic (MHD) hybrid nanoliquid Au-Cu/Blood over a permeable, porous stretched cylindrical surface. Blood is considered as a Newtonian liquid since it exhibits Newtonian properties in big cavities, arteries and blood veins. The influence of essential governing parameters, including the concentration-to-thermal buoyancy forces ratio; mixed convection parameter; activation energy; Hartmann number; Darcy number; radiation, heat source/sink, and chemical reaction parameters; Eckert number; Schmidt number on temperature, velocity and concentration distributions are inspected. The analytical findings are presented through two-dimensional graphical illustrations and tabular representations.

Figures 2-4 reveal the impact of the mixed convection $(\lambda)$ parameter on the velocity $(f^{'}(\eta))$, temperature $(\theta(\eta))$ and concentration $(\phi(\eta))$ profiles of the hybrid nanoliquid $Au - Cu$/Blood flow. As $\lambda$ grows, $f^{'}(\eta)$ rises, whereas $\phi(\eta)$ and $\theta(\eta)$ profiles decrease. The mixed convection factor defines the ratio between viscous and buoyancy forces. As $\lambda$ increases, buoyancy forces become more dominant over viscous resistance, causing an increase in the velocity distribution of blood-based hybrid nanoliquid. This acceleration enhances mixing and advection, leading to a dilution effect that lowers the solute concentration. Consequently, the concentration border layer becomes thinner, further decreasing the concentration distribution. Moreover, greater temperature variations generate stronger buoyancy forces, which improve convective heat transfer. This enhanced convection facilitates heat dissipation, lowering the liquid temperature. As the consequence, the temperature boundary layer becomes thinner, signifying more efficient heat removal.

Figures 5 and 6 elucidate the effect of the concentration-to-thermal buoyancy forces ratio parameter $(N)$ on $f^{'}(\eta)$ and $\phi(\eta)$ profiles of $Au-Cu$/Blood hybrid nanofluid. Higher $N$ increases $f^{'}(\eta)$ profile while decreasing the $\phi(\eta)$ profile. Since $N$ signifies the ratio between thermal and concentration buoyancy pressures, a greater $N$ results in an intensified concentration buoyancy pressure, therefore improves the velocity profile of liquid. The concentration profile declines as $N$ increases because a higher ratio indicates that the buoyancy force resulting from concentration differences becomes relatively weaker compared to the buoyancy force generated by temperature variations. Consequently, its influence on the concentration distribution within the fluid diminishes.

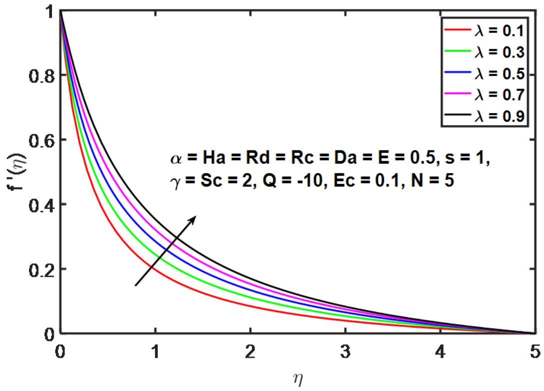


FIGURE 2. Impacts of different values of $\lambda$ (mixed convection parameter) on $f^{'}(\eta)$.

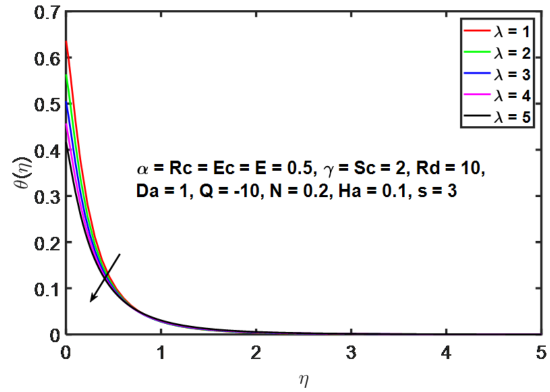


FIGURE 3. Impressions of diverse values of $\lambda$ (mixed convection parameter) on $\theta(\eta)$.

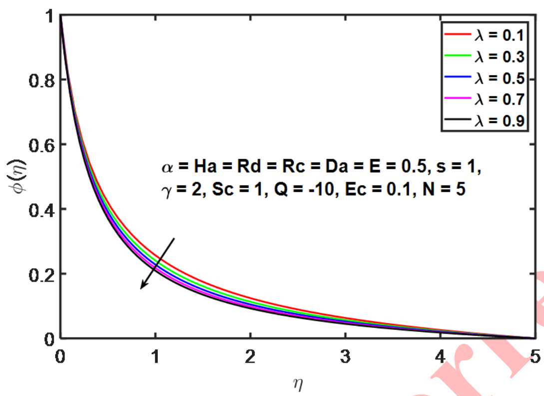


FIGURE 4. Impacts of different values of $\lambda$ (mixed convection parameter) on $\phi(\eta)$.

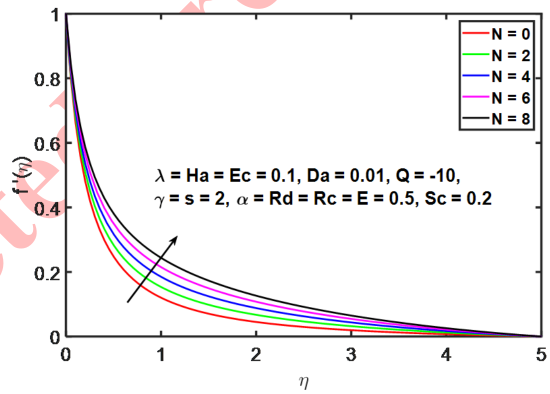


FIGURE 5. Impressions of diverse values of $N$ (concentration-to-thermal buoyancy ratio) on $f^{'}(\eta)$.



Figures 7-9 depict the impact of the activation energy ($E$), chemical reaction ($Rc$) and Schmidt number ($Sc$) on $\phi(\eta)$. As $E$ increases, $\phi(\eta)$ profile rises accordingly, however, an opposite tendency appears with the growth of $Rc$ and $Sc$. Rise in $E$ slows down the reaction rate, decreasing nanoparticle consumption and enabling a higher concentration of the hybrid nanofluid to be maintained, which enhances the concentration profile. Higher $Rc$ increases the destructive chemical reaction rate, leading to a smaller solute surface layer and enhanced mass transfer, which significantly decreases the concentration profile. $Sc$ signifies the ratio between mass and momentum diffusivities in liquid flowing. Greater Sc indicates increased momentum diffusion compared to mass diffusion, causing a decline in the concentration pattern of blood-based hybrid nanofluid. During disease therapy, these three parameters are utilized to regulate blood flowing concentration via stenosis arteries, excellently reducing the risk of heart failure [33].

Figures 10-12 demonstrate the influence of curvature parameter ($\gamma$) on $f^{'}(\eta)$, $\phi(\eta)$ and $\theta(\eta)$ profiles. As $\gamma$ upsurges, the profiles $f^{'}(\eta)$, $\theta(\eta)$ and $\phi(\eta)$ show a rising trend. When $\gamma$ is large, it signifies a reduction in the radius of the cylinder, which minimizes the interaction area between the boundary layer and blood-based hybrid nanofluid. As the consequence, the surface's resistive force on the liquid lessens, causing an increase in the $f^{'}(\eta)$ profile. Additionally, a

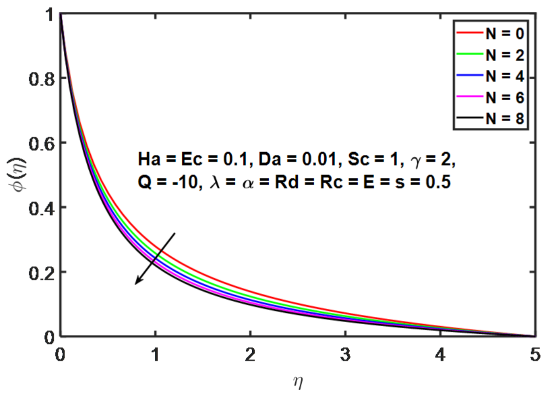


FIGURE 6. Impressions of diverse values of $N$ (concentration-to-thermal buoyancy ratio) on $\phi(\eta)$.

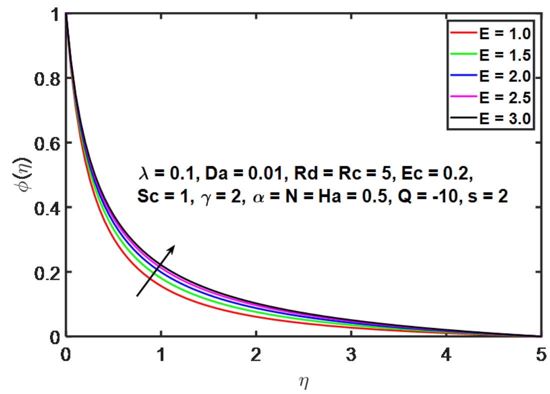


FIGURE 7. Impressions of diverse values of $E$ (activation energy parameter) on $\phi(\eta)$.

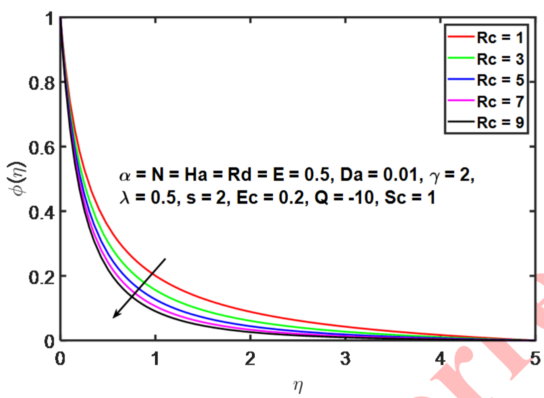


FIGURE 8. Impacts of different values of $Rc$ (chemical reaction parameter) on $\phi(\eta)$.

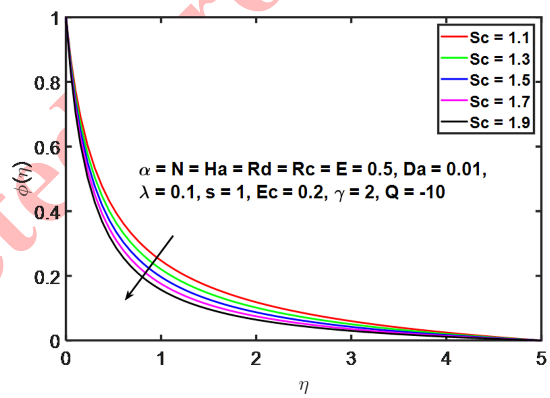


FIGURE 9. Impressions of diverse values of $Sc$ (Schmidt number) on $\phi(\eta)$.



reduced contact surface limits heat transfer from the cylinder to the surrounding liquid, thereby expanding the thermal boundary layer and elevating the temperature profile. Given the inverse correlation between curvature parameter and viscosity, the concentration distribution rises as $\gamma$ upturns.

Figures 13 and 14 demonstrate the effect of Hartmann ($Ha$) number on the velocity and temperature profiles. As the values of $Ha$ increases, $f^{'}(\eta)$ decreases and $\theta(\eta)$ increases. The reduction in $f^{'}(\eta)$ occurs owing to the interaction between the blood flowing and magnetic field, which induces an opposing force called the Lorentz force, impeding the movement of blood-based hybrid nanofluid. Meanwhile, the temperature distribution rises with the magnetic field restricts fluid motion, thereby diminishing convective heat transfer and creating a sharper temperature gradient. This research highlights the capability of magnetic fields to regulate blood flowing within arteries, presenting them as a promising approach for managing cardiovascular diseases. High-intensity magnetic fields are widely employed in MRI scans, facilitating faster fracture curative, supporting nerve regeneration, and offering various other medical advantages. Therefore, investigating blood flowing dynamics under the effect of a strong magnetic field holds significant scientific and medical value [13, 14].

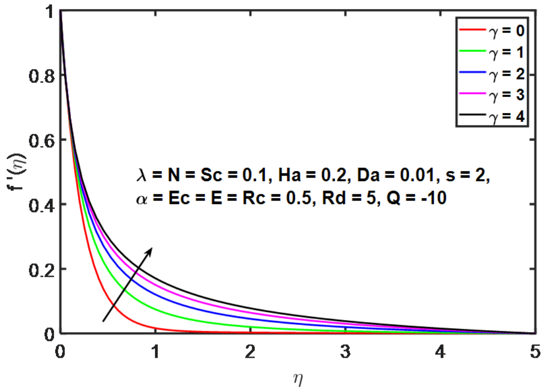


FIGURE 10. Impacts of different values of $\gamma$ (curvature parameter) on $f^{'}(\eta)$.

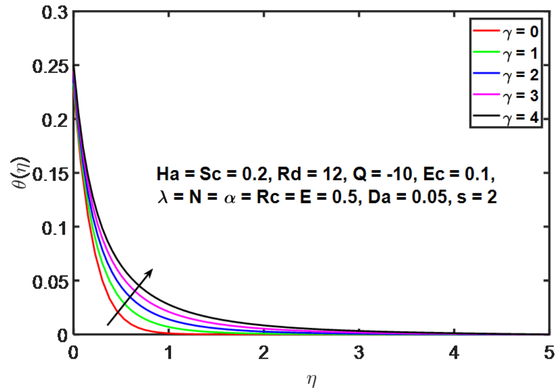


FIGURE 11. Impacts of different values of $\gamma$ (curvature parameter) on $\theta(\eta)$.

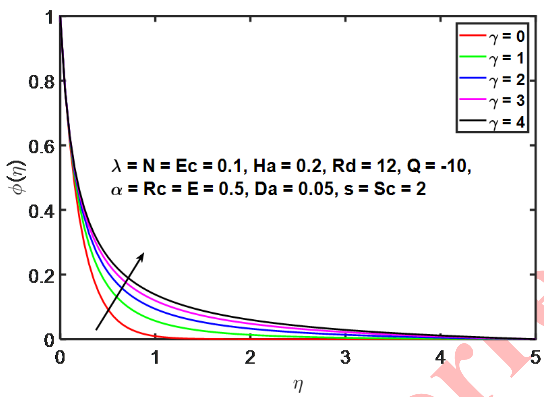


FIGURE 12. Impressions of diverse values of $\gamma$ (curvature parameter) on $\phi(\eta)$.

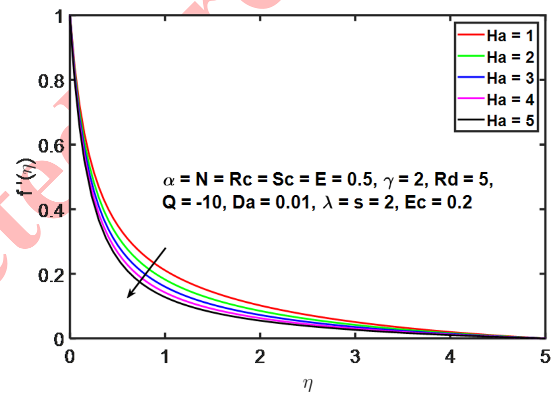


FIGURE 13. Impressions of diverse values of $Ha$ (Hartmann number) on $f^{'}(\eta)$.



Figures 15 and 16 show the impact of Darcy ($Da$) number on $f^{'}(\eta)$ and $\theta(\eta)$ profiles. As the values of $Da$ increases, $f^{'}(\eta)$ decreases and $\theta(\eta)$ increases. Darcy number represents the porous medium's penetrability, how easily fluid can traverse through it. An escalation in $Da$ influences the penetrability within the porosity framework, leading to a reduction in the velocity distribution. As $Da$ rises, improved permeability supports fluid motion and boosts heat transfer, ultimately resulting in a higher temperature distribution.

Figures 17-19 show the impact of the radiation ($Rd$) parameter, Eckert ($Ec$) number and heat source/sink ($Q$) parameter on $\theta(\eta)$ profile of $Au-Cu$/Blood hybrid nanofluid. As $Rd$, $Ec$ and $Q$ grow, so does $\theta(\eta)$ profile. Due to the opposite relationship between thermal conductivity and radiation, along with the additional thermal energy generated, $\theta(\eta)$ increases as $R$ rises. This highlights the significance of $R$ in regulating temperature distribution. The findings have practical implications across various fields, including the design of drug delivery systems utilizing magnetically controlled nano sized particles for treating injured arteries and the assessment of heat variations in hyperthermia therapy for cancer treatment. For instance, in the presence of pathological conditions, a higher radiation dose could support surgeons in elevating the temperature distribution to destroy cells with cancer while minimizing harm to

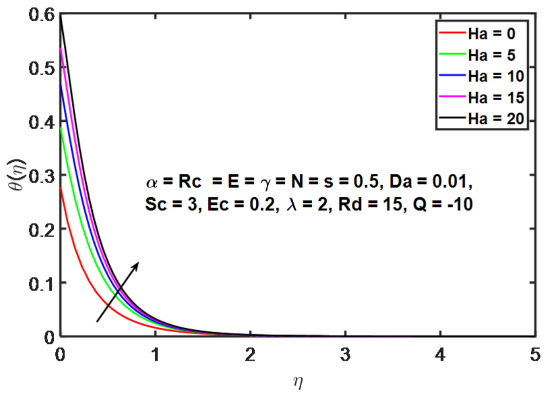


FIGURE 14. Impacts of different values of $Ha$ (Hartmann number) on $\theta(\eta)$.

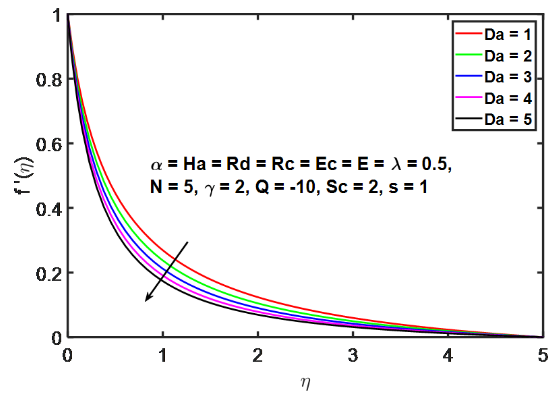


FIGURE 15. Impacts of different values of $Da$ (Darcy number) on $f^{'}(\eta)$.

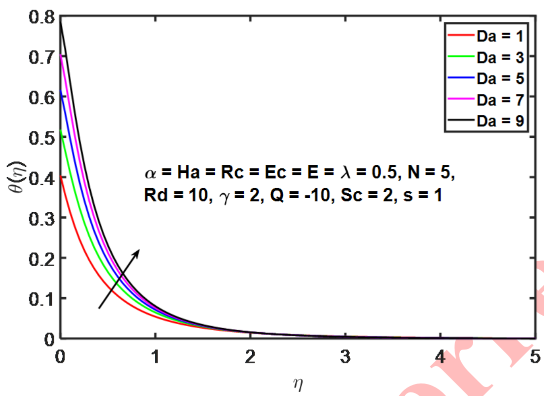


FIGURE 16. Impacts of different values of $Da$ (Darcy number) on $\theta(\eta)$.

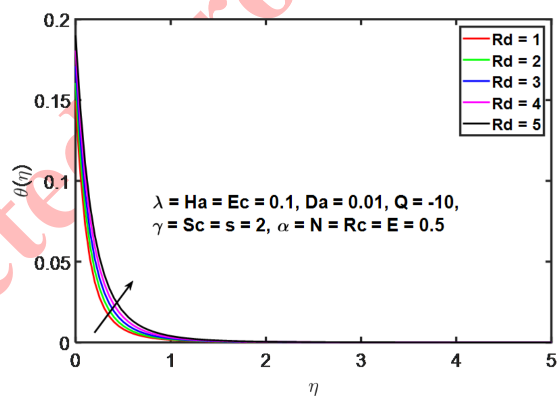


FIGURE 17. Impressions of diverse values of $Rd$ (radiation parameter) on $\theta(\eta)$.



good tissue [55]. Ec is a quantity without dimensions represents the ratio between thermal energy and kinetic energy in a liquid flow. An upsurge in Ec signifies that the kinetic energy is higher in comparison to the liquid's thermal energy. This enhances heat transfer efficiency and improves the nanofluid's cooling performance. As Ec rises, friction between neighboring fluid layers generates internal energy, leading to the alteration of mechanical energy into thermal energy, which subsequently elevates the fluid temperature. The presence of a heat source enhanced through a heat absorption/generation device, increases the liquid's energy, resulting in a thicker thermal boundary layer.

During the computation of $\sqrt{Re}C_f$ (skin friction coefficient), $Re^{-\frac{1}{2}}Nu$ (Nusselt number) and $Re^{-\frac{1}{2}}Sh$ (Sherwood number), following parameters with stated values were used: $\phi_2 = \phi_1 = \gamma = Rd = Sc = Q = s = 0.1$, $\lambda = \alpha = N = Ha = E = 0.5$, $Ec = Rc = 0.2$, $Da = 0.01$. While calculating $\sqrt{Re}C_f$, $Re^{-\frac{1}{2}}Nu$ and $Re^{-\frac{1}{2}}Sh$ for a single parameter, all other parameters remain unchanged.

Table 3 presents data illustrating the influence of $\sqrt{Re}C_f$, $Re^{-\frac{1}{2}}Nu$ and $Re^{-\frac{1}{2}}Sh$ on the key dimensionless parameters $\lambda, E, Rc, Ha$ and $Rd$ in this work. An upsurge in $\lambda, E$ and $Rd$ leads to a perceptible rise in $\sqrt{Re}C_f$, whereas variations in $Rc$ and $Ha$ result in a diminution. $Re^{-\frac{1}{2}}Nu$ declines with increasing values of $Rc$ and $Ha$, whereas

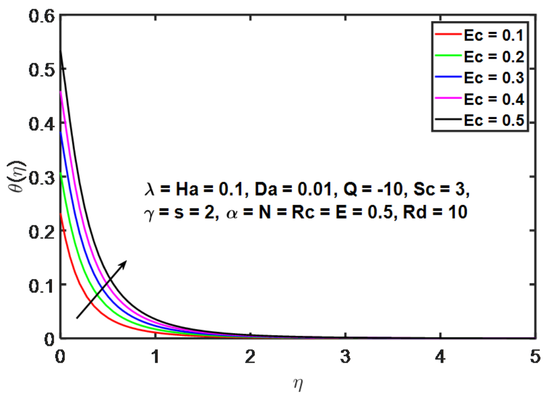


Figure 18. Impacts of different values of $Ec$ (Eckert number) on $\theta(\eta)$.

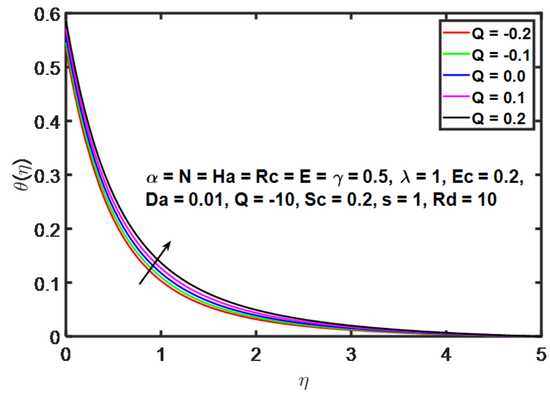


Figure 19. Impacts of different values of $Q$ (heat source/sink parameter) on $\theta(\eta)$.



it exhibits an upward trend with increasing $\lambda, E$ and $Rd$. $Re^{-\frac{1}{2}}Sh$ increases as $E$ and $Ha$ rise, while it declines with growing $\lambda, Rc$ and $Rd$ values. In this study, it is also observed that as $\lambda$ varies from 0.1 to 0.7, $\sqrt{Re}C_f$ and $Re^{-\frac{1}{2}}Nu$ values increase by 27% and 30%, respectively, while $Re^{-\frac{1}{2}}Sh$ decreases by 8%. When $E$ varies from 1.0 to 2.5, $\sqrt{Re}C_f$,$Re^{-\frac{1}{2}}Nu$ and $Re^{-\frac{1}{2}}Sh$ increase by 0.1%, 0.1%, and 1.4%, respectively. As $Rc$ increases from 1 to 7, $\sqrt{Re}C_f$,$Re^{-\frac{1}{2}}Nu$ and $Re^{-\frac{1}{2}}Sh$ decrease by 3%, 3.4%, and 57%, respectively. When $Rd$ varies from 0.1 to 0.4, $\sqrt{Re}C_f$,$Re^{-\frac{1}{2}}Nu$ increase by 0.3% and 13%, respectively, while the $Re^{-\frac{1}{2}}Sh$ decreases by 0.04%. Finally, as Ha increases from 1 to 4, $\sqrt{Re}C_f$,$Re^{-\frac{1}{2}}Nu$ decrease by 48% and 50%, respectively, whereas $Re^{-\frac{1}{2}}Sh$ increases by 8%. Table 4 explores how the mixed effects of the curvature and Darcy numbers effects the skin friction coefficient, using parameters $s = -30$, $Ha = 1$, $Pr = 8$, $Rd = 1$, $Q = -1$, $Ec = 1$ (from [43]). The findings show that converting a stretchy porous surface into a stretchy porous cylinder, especially in the process of conditions of elevated fluid injection and Darcy forces, sparks a slight increase on Additionally, this coefficient further progresses as the medium's permeability over the cylinder's surface is enhanced. Table 5, using the same parameter settings (with the exception of $Rd$, set here as $Rd = 0$), examines local Nusselt number with similar effects. The results reveal that rates of heat transfer increase with a higher curvature parameter, particularly in scenarios involving high fluid injection, heat absorption, minimum magnetic field force, and increasing Eckert numbers. However, a rise in medium permeability reduces for both cylinder and the porous stretchy sheet reduces to the local Nusselt number. Together, these findings align well with an outcomes followed by Sadighi et al. [43].

## 5. Conclusions

This study investigates the behaviour of a two dimensional, axisymmetric, steady-state, incompressible, viscous, laminar MHD $Au-Cu$/blood hybrid nanoliquid flowing on a permeable, porous, stretched cylinder. The effects of the mixed convection parameter ($0.1 \leq \lambda \leq 5$), ratio of concentration-to-thermal buoyancy forces ($0 \leq N \leq 8$), activation energy ($1 \leq E \leq 3$), chemical reaction ($1 \leq Rc \leq 9$), Schmidt number ($1.1 \leq Sc \leq 1.9$), curvature parameter ($0 \leq \gamma \leq 4$), Hartmann number ($0 \leq Ha \leq 20$), Darcy number ($1 \leq Da \leq 9$), radiation parameter ($1 \leq Rd \leq 5$), Eckert number ($0.1 \leq Ec \leq 0.5$), heat source/sink parameter ($-0.2 \leq Q \leq 0.2$) on the temperature, velocity and concentration distributions of $Au-Cu$/Blood hybrid nanoliquid are analysed. Tiwari-Das model [42] is performed to investigate the flow behaviour. Fluid flowing equations are elucidated with the BVP-5C shooting technique in MATLAB. This model has been thoroughly validated with existing data and has shown outstanding accuracy. Based on this analytical investigation, the primary outcomes are follows:

TABLE 3. $\sqrt{Re}C_{fx}$, $Re^{-\frac{1}{2}}Nu_x$ and $Re^{-\frac{1}{2}}Sh_x$ impacts on the $Au - Cu/Blood$ hybrid nanofluid.

| $\lambda$ | $E$ | $Rc$ | $Rd$ | $Ha$ | $\sqrt{Re}C_{fx}$ | $Re^{-\frac{1}{2}}Nu_x$ | $Re^{-\frac{1}{2}}Sh_x$ |
|---|---|---|---|---|---|---|---|
| 0.1 | – | – | – | – | -2.786887 | 3.466970 | -0.468558 |
| 0.3 | – | – | – | – | -2.514282 | 3.824058 | -0.483616 |
| 0.5 | – | – | – | – | -2.265907 | 4.165565 | -0.496561 |
| 0.7 | – | – | – | – | -2.034669 | 4.494542 | -0.508059 |
| – | 1.0 | – | – | – | -2.264621 | 4.168448 | -0.491300 |
| – | 1.5 | – | – | – | -2.263823 | 4.170232 | -0.487995 |
| – | 2.0 | – | – | – | -2.263331 | 4.171333 | -0.485923 |
| – | 2.5 | – | – | – | -2.263027 | 4.172011 | -0.484626 |
| – | – | 1.0 | – | – | -2.278462 | 4.137539 | -0.550308 |
| – | – | 3.0 | – | – | -2.304683 | 4.079301 | -0.669298 |
| – | – | 5.0 | – | – | -2.325517 | 4.033431 | -0.772118 |
| – | – | 7.0 | – | – | -2.342590 | 3.996199 | -0.863445 |
| – | – | – | 0.1 | – | -2.265907 | 4.165565 | -0.496561 |
| – | – | – | 0.2 | – | -2.263563 | 2.533012 | -0.496635 |
| – | – | – | 0.3 | – | -3.380217 | 2.048726 | -0.456117 |
| – | – | – | 0.4 | – | -2.258879 | 1.736706 | -0.496785 |
| – | – | – | – | 1 | -2.524880 | 3.401293 | -0.485804 |
| – | – | – | – | 2 | -2.981936 | 2.533012 | -0.468813 |
| – | – | – | – | 3 | -3.380217 | -3.380217 | -0.456117 |
| – | – | – | – | 4 | -3.736930 | 1.736706 | -0.446276 |

TABLE 4. Comparison of $C_f Re_x^{\frac{1}{2}}$ values with the results of Sadighi et al. [43].

| $Da$ | Sadighi *et al.*, [43] | | | Current Study | | |
|---|---|---|---|---|---|---|
| | $\gamma = 0$ | $\gamma = 0.001$ | $\gamma = 0.002$ | $\gamma = 0$ | $\gamma = 0.001$ | $\gamma = 0.002$ |
| 0.5 | -0.083103 | -0.083108 | -0.083114 | -0.083103 | -0.083109 | -0.083114 |
| 0.6 | -0.086417 | -0.086423 | -0.086429 | -0.086418 | -0.086423 | -0.086429 |
| 0.7 | -0.089731 | -0.089737 | -0.089743 | -0.089732 | -0.089738 | -0.089743 |

TABLE 5. Comparing of local Nusselt number $(Re_x^{-1/2}Nu_x)$ with Sadighi et al. [43].

| $Da$ | Sadighi *et al.*, [43] | | | Current Study | | |
|---|---|---|---|---|---|---|
| | $\gamma = 0$ | $\gamma = 0.001$ | $\gamma = 0.002$ | $\gamma = 0$ | $\gamma = 0.001$ | $\gamma = 0.002$ |
| 0.5 | 0.095129 | 0.095130 | 0.095131 | 0.095173 | 0.095174 | 0.095175 |
| 0.6 | 0.094825 | 0.094826 | 0.094827 | 0.094870 | 0.094871 | 0.094871 |
| 0.7 | 0.094524 | 0.094525 | 0.094526 | 0.094569 | 0.094569 | 0.094570 |

- As $\lambda$ increases, the velocity profile $f^{'}(\eta)$ exhibits an upward trend, whereas the concentration profile $\phi(\eta)$ and temperature distribution $\theta(\eta)$ show a decline. When $\lambda$ varies from 0.1 to 0.7, $\sqrt{Re}C_f$ (skin friction coefficient) and $Re^{-\frac{1}{2}}Nu$ (heat transfer rate) rise by 27% and 30% respectively, while $Re^{-\frac{1}{2}}Sh$ (mass transfer rate) decreases by 8%.

- As $E$ increases, the concentration profile $\phi(\eta)$ rises, whereas higher values of $Rc$ and $Sc$ exhibit a declining trend. When $E$ ranges from 1.0 to 2.5, $\sqrt{Re}C_f$, $Re^{-\frac{1}{2}}Nu$ and $Re^{-\frac{1}{2}}Sh$ show increments of 0.1%, 0.1%, and 1.4% respectively. Conversely, as $Rc$ increases from 1 to 7, $\sqrt{Re}C_f$, $Re^{-\frac{1}{2}}Nu$ and $Re^{-\frac{1}{2}}Sh$ decline by 3%, 3.4% and 57%, respectively.

- As $Ha$ increases $f^{'}(\eta)$ profile declines, while $\theta(\eta)$ profile exhibits an ascendant trend. When Ha varies from 1 to 4, $\sqrt{R}eC_f$ and $Re^{-\frac{1}{2}}Nu$ decrease by 48% and 50%, respectively.

- As $Rd$, $Ec$ and $Q$ increase, the temperature profile also rises. When $Rd$ ranges from 0.1 to 0.4, $\sqrt{R}eC_f$ and $Re^{-\frac{1}{2}}Nu$ increase by 0.3% and 13% respectively, while $Re^{-\frac{1}{2}}Sh$ decreases by 0.04%.

- An upsurge in $N$ enhances the velocity profile, whereas the concentration profile diminishes. As $\gamma$ rises, temperature profile, velocity distribution and concentration profiles exhibit a rising trend. Meanwhile, as $Da$ increases, the velocity distribution declines, whereas the temperature profile shows a rising tendency.

## References


[1] N. Abbas, S. Nadeem, A. Saleem, M. Y. Malik, A. Issakhov, and F. M. Alharbi, *Models base study of inclined MHD of hybrid nanofluid flow over nonlinear stretching cylinder*, Chinese Journal of Physics, *69* (2021), 109-117.

[2] P. Agarwal, G. Wang, and M. Al-Dhaifallah, *Fractional calculus operators and their applications to thermal systems*, Advances in Mechanical Engineering, *10*(2018).

[3] A. Ali, T. Kanwal, and M. Awais, et al., *Impact of thermal radiation and non-uniform heat flux on MHD hybrid nanofluid along a stretching cylinder*, Sci Rep, *11* (2021), 20262.

[4] I. Alraddadi, A. Ayub, S. M. Hussain, U. Khan, S. Z. H. Shah, and A. M. Hassan, *The significance of ternary hybrid cross bio-nanofluid model in expanding/contracting cylinder with inclined magnetic field*, Front. Mater, *10* (2023), 1242085.

[5] M. Akram, W. Jamshed, B. Shankar Goud, A. A. Pasha, T. Sajid, M. M. Rahman, M. Arshad, and W. Weera, *Irregular heat source impact on carreau nanofluid flowing via exponential expanding cylinder: A thermal case study*, Case Studies in Thermal Engineering, *36* (2022), 102171.

[6] A. U. Awan, B. Ali, S. A. A. Shah, M. Oreijah, K. Guedri, and S. M. Eldin, *Numerical analysis of heat transfer in Ellis hybrid nanofluid flow subject to a stretching cylinder*, Case Studies in Thermal Engineering, *49* (2023), 103222.

[7] W. F. W. Azmi, A. Q. Mohamad, L. Y. Jiann, et al, *Unsteady natural convection flow of blood Casson nanofluid (Au) in a cylinder: nano-cryosurgery applications*, Sci Rep, *13* (2023), 5799.

[8] M. A. Basit, U. Farooq, M. Imran, N. Fatima, A. Alhushaybari, S. Noreen, S. M. Eldin, and A. Ali, *Comprehensive investigations of (Au-Ag/Blood and Cu-Fe3O4/Blood) hybrid nanofluid over two rotating disks: Numerical and computational approach*, Alexandria Engineering Journal, *72* (2023) 19-36.

[9] H. T. Basha, K. Rajagopal, N. A. Ahammad, S. Sathish, and G. Sreedhara Rao, *Finite Difference Computation of Au-Cu/Magneto-Bio-Hybrid Nanofluid Flow in an Inclined Uneven Stenosis Artery*, Complexity, (2022), 2078372.

[10] R. Chinmoy and A. Nayak, *MHD nonlinear thermally radiative $Ag-TiO_2/H_2O$ hybrid nanofluid flow over a stretching cylinder with Newtonian heating and activation energy*, Physica Scripta, *99* (2024), 085201.

[11] S. A. Conrad and D. Wang, *Evaluation of recirculation during venous extracorporeal membrane oxygenation using computational fluid dynamics incorporating fluid-structure interaction*, Asaio J., *67* (2021), 943–953.

[12] S. Das, H. Mondal, and K. Prabir Kumar, *Flow Analysis of Mixed Convective Nanofluid Flow in Presence of Magnetic Field with Thermal Radiation and Heat Source/Sink*, Journal of Nanofluids, *12* (2023), 1008–1016.

[13] S. Das, T. K. Pal, and R. N. Jana, *Outlining impact of hybrid composition of nanoparticles suspended in blood flowing in an inclined stenosed artery under magnetic field orientation*, Bio Nano Sci., *11* (2021) 99–115.

[14] S. Das, T. K. Pal, R. N. Jana, and B. Giri, *Significance of Hall currents on hybrid nano-blood flow through an inclined artery having mild stenosis: Homotopy perturbation approach*, Microvascular Research, *137* (2021) 104192.

[15] Y. Dharmendar Reddy, B. Shankar Goud, K. S. Nisar, B. Alshahrani, M. Mahmoud, and C. Park, *Heat absorption/generation effect on MHD heat transfer fluid flow along a stretching cylinder with a porous medium*, Alexandria Engineering Journal, *64* (2023), 659-666.

[16] M. Gholinia, M. Armin, A. A. Ranjbar, and D. D. Ganji, *Numerical thermal study on CNTs/ C2H6O2– H2O hybrid base nanofluid upon a porous stretching cylinder under impact of magnetic source*, Case Studies in Thermal Engineering, *14* (2019), 100490.

[17] P. Guo, Y.Leng, F. Nazir, J. Ahmed, A. Mohamed, I. Khan, and I. E. Elseesy, *Mixed convection phenomenon for hybrid nanofluid flow exterior to a vertical spinning cylinder with binary chemical reaction and activation energy*, Case Studies in Thermal Engineering, *54* (2024), 103943.

[18] R. J. P. Gowda, R. Naveen Kumar, and B. C. Prasannakumara, *Two-Phase Darcy-Forchheimer Flow of Dusty Hybrid Nanofluid with Viscous Dissipation Over a Cylinder*, Int. J. Appl. Comput. Math, *7* (2021).

[19] I. Hammami, M. Nadiyah, A. A. A. Jomaa, and M. kamoun, *Gold nanoparticles: Synthesis properties and applications*, Journal of King Saud University - Science, *33* (2021), 101560.

[20] T. Hayat and S. Nadeem, *Heat transfer enhancement with Ag–CuO/water hybrid nanofluid*, Results in Physics, *7* (2017), 2317–2324.

[21] A. Hussain, L. Sarwar, A. Rehman, S. Akbar, F. Gamaoun, H. H. Coban, A. H. Almaliki, and M. S. Alqurashi, *Heat Transfer Analysis and Effects of (Silver and Gold) Nanoparticles on Blood Flow Inside Arterial Stenosis*, Applied Sciences, *12* (2022), 1601.

[22] I. Imoro, C. J. Etwire, and R. Musah, *MHD flow of blood-based hybrid nanofluid through a stenosed artery with thermal radiation effect*, Case Studies in Thermal Engineering, *59* (2024), 104418.

[23] H. Jassim, H. Ahmad, A. Shamaoon, and C. Cesarano, *An Efficient Hybrid Technique for the Solution of Fractional-Order Partial Differential Equations*, Carpathian Math. Publ., *13* (2021), 790-804.

[24] J. P. Joule, *On the production of heat by voltaic electricity*, In Abstr. Pap. Print. Philos.Trans. R. Soc., 280–282.

[25] S. Kavya and V. Nagendramma, *Opposing and assisting flow of a hybrid Newtonian/non-Newtonian nanofluid past a stretching cylinder*, Journal of Mines, Metals and Fuels, *71* (2023), 1045–1057.

[26] N. S.Khashi'ie, N. M. Arifin, I.Pop, and N. S. Wahid, *Flow and heat transfer of hybrid nanofluid over a permeable shrinking cylinder with Joule heating: A comparative analysis*, Alexandria Engineering Journal, *59* (2020), 1787-1798.

[27] Y. J. Lim, S. Shafie, S. M. Isa, N. A. Rawi, and A. Q. Mohamad, *Impact of chemical reaction, thermal radiation and porosity on free convection Carreau fluid flow towards a stretching cylinder*, Alexandria Engineering Journal, *61* (2022), 4701-4717.

[28] S. Li, N. Shahmir, M. Ramzan, N. A. Ahammad, A. M. S. Alhuthali, and C. A. S. S. Kadry, *Thermal inspection of hybrid nanofluid flows over a stretched cylinder at an oblique stagnation point with variable characteristics*, Z Angew Math Mech., *104* (2024), e202300837.

[29] A. Majeed, M. Zubair, A. Khan, T. Muhammad, and M. Alqarni, *Significance of Thermophoretic and Brownian Motion on MHD Nanofluids Flow towards a Circular Cylinder under the Inspiration of Multiple Slips: An Industrial Application*, Mathematical Problems in Engineering, (2021), 8634185.

[30] Z. Mahmood, S. E. Alhazmi, A. Alhowaity, et al., *MHD mixed convective stagnation point flow of nanofluid past a permeable stretching sheet with nanoparticles aggregation and thermal stratification*, Sci Rep, *12* (2022), 16020.

[31] Ch. Maheswari, R. Mohana Ramana, G. Balaji Prakash, D. Ramesh, and D. Vijaya Kumar, *Influence of thermophoresis and Brownian motion on MHD hybrid nanofluid MgO-Ag/H2O flow along moving slim needle*, Journal of Advanced Research in Applied Sciences and Engineering Technology, *36* (2023), 67–90.

[32] J. Madhukesh, G. Ramesh, R. Varun Kumar, and B. Prasannakumara, *Assessment of Arrhenius activation energy in stretched flow of nanofluid over a rotating disc*, Heat Transfer, *50* (2021), 2807–2828.

[33] G. Mandal and D. Pal, *Impacts of binary chemical reaction with activation energy on MHD thermally radiating blood based hybrid nanofluid flow through shrinking-stenotic artery: Entropy generation and stability analysis*, Hybrid Advances, *7* (2024), 100293.

[34] H. Mondal, S. Das, and K. Prabir Kumar, *Influence of an inclined stretching cylinder over MHD mixed convective nanofluid flow due to chemical reaction and viscous dissipation*, Heat Transfer, *49* (2020), 1–11.

[35] R. Mohana Ramana, C. Maheswari, S. Mohiddin Shaw, G. Dharmaiah, U. F. Gamiz, and S. Noeiaghdam, *Numerical investigation of 3-D rotating hybrid nanofluid Forchheimer flow with radiation absorption over a stretching sheet*, Results in Engineering, *22* (2024), 102019.

[36] K. S. Mekheimer, A. Z. Zaher, and W. M. Hasona, *Entropy of AC electro-kinetics for blood mediated gold or copper nanoparticles as a drug agent for thermotherapy of oncology*, Chinese Journal of Physics, *65* (2020), 123-138.

[37] A. Mishra and M. Kumar, *Velocity and thermal slip effects on MHD nanofluid flow past a stretching cylinder with viscous dissipation and Joule heating*, SN Appl. Sci., *2* (2020), 1350.

[38] D. Mujahed, K. S. Nisar, A. Praveen, and E. Alaa, *Modeling and identification of heat exchanger process using least squares support vector machines*, Thermal Science, *21* (2017), 2859-2869.

[39] K. M. Nihaal, U. S. Mahabaleshwar, N. Swaminathan, D. Laroze, and I. V. Shevchuk, *A Numerical Investigation of Activation Energy Impact on MHD Water-Based Fe3O4 and CoFe2O4 Flow between the Rotating Cone and Expanding Disc.* Mathematics, *12* (2024), pp.2530.

[40] N.C. Roy and A. Akter, *Dual solutions of mixed convective hybrid nanofluid flow over a shrinking cylinder placed in a porous medium*, Heliyon, *9* (2023), e22166.

[41] T. Salahuddin, *Carreau fluid model towards a stretching cylinder: Using Keller box and shooting method*, Ain Shams Engineering Journal, *11* (2020), 495-500.

[42] S. Sadighi, M. Jabbari, H. Afshar, H. Ahmadi, and A. Danesh, *MHD heat and mass transfer nanofluid flow on a porous cylinder with chemical reaction and viscous dissipation effects: Benchmark solutions*, Case Studies in Thermal Engineering, *40* (2022), 102443.

[43] S. Sadighi, H. Afshar, H. A. D. Ashtiani, and M. Jabbari, *MHD flow and conductive heat transfer on a permeable stretching cylinder: Benchmark solutions*, Case Studies in Thermal Engineering, *44* (2023), 102886.

[44] M. Sharma, B. K. Sharma, U. Khanduri, N. K. Mishra, S. Noeiaghdam, and U. F. Gamiz, *Optimization of heat transfer nanofluid blood flow through a stenosed artery in the presence of Hall effect and hematocrit dependent viscosity*, Case Studies in Thermal Engineering, *47* (2023), 103075.

[45] F. Shahzad, W. Jamshed, F. Aslam, R. Bashir, E. S. M. Tag El Din, H. A. E. Khalifa, and A. M. Alanzi, *MHD Pulsatile Flow of Blood-Based Silver and Gold Nanoparticles between Two Concentric Cylinders*, Symmetry, *14* (2022), 2254.

[46] F. H. Sohut, U. Khan, A. Ishak, S. K. Soid, and I. Waini, *Mixed Convection Hybrid Nanofluid Flow Induced by an Inclined Cylinder with Lorentz Forces*, Micro machines, *14* (2023), 982.

[47] B. Souayeh, K. Ramesh, N. Hdhiri, E. Yasin, M. W. Alam, K. Alfares, and A. Yasin, *Heat Transfer Attributes of Gold–Silver–Blood Hybrid Nanomaterial Flow in an EMHD Peristaltic Channel with Activation Energy*, Nanomaterials, *12* (2022), 1615.

[48] S. Suneetha, K. Subbarayudu, and A. R. P. Bala, *Hybrid nanofluids development and benefits: A comprehensive review*, J. Ther. Eng., *8* (2022), 445–455.

[49] J. Tripathi, B. Vasu, and O. Anwar Bég, *Computational simulations of hybrid mediated nano- hemodynamics (Ag-Au/Blood) through an irregular symmetric stenosis*, Computers in Biology and Medicine, *130* (2021), 104213.

[50] C. Umadevi, M. Dhange, B. Haritha, and T. Sudha, *Flow of blood mixed with copper nanoparticles in an inclined overlapping stenosed artery with magnetic field*, Case Studies in Thermal Engineering, *25* (2021), 100947.

[51] K. Venkateswara Raju, C. Maheswari, R. Mohana Ramana, S. Vijayakumar Varma, and M. Changal Raju, *Comparative numerical study between MHD Forchheimer nano and hybrid nanofluid flows over stretching sheet under aligned magnetic field in the presence of radiation absorption*, International Journal of Modelling and Simulation, (2024), 1–18.

[52] A. Vodyashkin, A. Stoinova, and P. Kezimana, *Promising biomedical systems based on copper nanoparticles: Synthesis, characterization, and applications*, Colloids and Surfaces B: Biointerfaces, *237* (2024), 113861.

[53] W. F. Xia, S. Ahmad, M. Naveed Khan, H. Ahmad, A. Rehman, J. Baili, and T. N. Gia, *Heat and mass transfer analysis of nonlinear mixed convective hybrid nanofluid flow with multiple slip boundary conditions*, Case Studies in Thermal Engineering, *32* (2022), 101893.

[54] H. Yasmin, L. A. AL-Essa, S. A. Lone, H. Alrabaiah, Z. Raizah, and A. Saeed, *Magnetohydrodynamic water-based hybrid nanofluid flow comprising diamond and copper nanoparticles on a stretching sheet with slips constraints*, Open Physics, *22* (2024), 20240007.

[55] S. B. Yaqoob, R. Adnan, R. M. Rameez Khan, and M. Rashid, *Gold, Silver, and Palladium Nanoparticles: A Chemical Tool for Biomedical Applications*, Front. Chem., *8* (2020), 376.